Production velocity of sea spray droplets

Edgar L Andreas,[1] Kathleen F. Jones,[2] and Christopher W. Fairall[3]

Received 9 June 2010; revised 7 September 2010; accepted 13 September 2010; published 28 December 2010.

[1] The sea spray generation function dF/dr_0 predicts the rate at which droplets of initial radius r_0 are produced at the sea surface. Because this function is not readily measurable in the marine environment, however, it is often inferred from measurements of the near-surface droplet concentration, $C(r_0)$, through an assumed velocity scale, the effective spray production velocity. This paper proceeds in reverse, though: It uses a reliable estimate of dF/dr_0 and 13 sets of measurements of $C(r_0)$ over the ocean to calculate the implied effective production velocity, V_{eff}, for droplets with initial radii r_0 from 5 to 300 μm. It then compares these V_{eff} values with four candidate expressions for this production velocity: the dry-deposition velocity, V_{Dh}; the mean wind speed at the significant wave amplitude ($A_{1/3}$), $U_{A_{1/3}}$; the standard deviation in vertical droplet velocity, σ_{wd}; and laboratory measurements of the ejection velocity of jet droplets, V_{ej}. The velocity scales $U_{A_{1/3}}$ and V_{ej} agree best with the implied V_{eff} values for $20 \le r_0 \le 300$ μm. The deposition velocity, V_{Dh}, which is the velocity most commonly used in this application, agrees worst with the V_{eff} values. For droplets with r_0 less than about 20 μm, the analysis also rejects the main hypothesis: that dF/dr_0 and $C(r_0)$ can be related through a velocity scale. These smaller droplets simply have residence times that are too long for spray concentrations to be in local equilibrium with the spray production rate.

Citation: Andreas, E. L, K. F. Jones, and C. W. Fairall (2010), Production velocity of sea spray droplets, *J. Geophys. Res.*, *115*, C12065, doi:10.1029/2010JC006458.

1. Introduction

[2] The rate at which sea spray droplets form remains illusive. Current estimates of that rate, especially for droplets larger than about 10 μm in radius, range over an order of magnitude [e.g., *Andreas*, 2002; *Lewis and Schwartz*, 2004, chap. 5]. The main reason for this uncertainty is that the spray generation function cannot be measured directly but must be inferred from its relation to quantities that can be measured [e.g., *Massel*, 2007, section 9.2].

[3] In our notation, the spray generation function is dF/dr_0; this gives the number of droplets of initial radius r_0 that pass upward through a unit horizontal area per second per micrometer increment in droplet radius [cf. *Monahan et al.*, 1986]. It has units of $m^{-2}\ s^{-1}\ \mu m^{-1}$.

[4] Spray production is closely associated with wave breaking and the resulting whitecap coverage. Although wave breaking is episodic and, thus, occurs over a small fraction of the ocean surface at any instant, dF/dr_0 is usually viewed as an area average. This definition is a necessary simplification because dF/dr_0 is useful in atmospheric models only as an area-averaged droplet flux.

[5] Although we assume that dF/dr_0 is the droplet flux at the sea surface, it is in essence an "effective" flux. Not all spray droplets that form are dynamically or thermodynamically important or can even be observed. These ineffectual droplets return almost instantaneously to the sea. See discussions of this distinction between total spray production and effective spray production by *Pattison and Belcher* [1999] and *Mueller and Veron* [2009b].

[6] One of the common reasons for interest in the spray generation function is that it provides the flux boundary condition at the bottom of the atmosphere in numerical studies that include marine aerosols [e.g., *Burk*, 1984; *Fairall et al.*, 1984; *Gong et al.*, 1997; *Massel*, 2007].

[7] A second reason is that analytical solutions of the conservation equation for droplets (and other particles) yield vertical concentration profiles of the form [e.g., *Goroch et al.*, 1980; *Fairall et al.*, 1990, 2009; *Kind*, 1992; *Hoppel et al.*, 2002]

$$C(z, r_0) = C(z_r, r_0)(z/z_r)^{-\beta}. \quad (1)$$

Here, C is the number concentration of droplets of radius r_0 (units $m^{-3}\ \mu m^{-1}$), z is the height, z_r is some reference height, and

$$\beta = \frac{V_g(r_0)}{k\ u_*}, \quad (2)$$

where $V_g(r_0)$ is the terminal fall speed of droplets of radius r_0, k (= 0.40) is the von Kármán constant, and u_* is the friction

[1]Seattle Division, NorthWest Research Associates, Inc., Lebanon, New Hampshire, USA.
[2]U.S. Army Cold Regions Research and Engineering Laboratory, Hanover, New Hampshire, USA.
[3]Physical Sciences Division, NOAA Earth System Research Laboratory, Boulder, Colorado, USA.

0148-0227/10/2010JC006458

velocity. Often, z_r is taken to be the roughness length z_0 [e.g., *Toba*, 1965; *Goroch et al.*, 1980]; hence, $C(z_r, r_0) = C(z_0, r_0) \equiv C_0(r_0)$ is the droplet concentration at the sea surface. As with dF/dr_0, $C_0(r_0)$ is assumed to be a horizontally averaged quantity.

[8] In turn, the following assumed relation between dF/dr_0 and C_0 is one of the most enduring in this field [e.g., *Moore and Mason*, 1954; *Toba*, 1965; *Fairall and Larsen*, 1984; *Andreas and DeCosmo*, 1999]:

$$dF/dr_0 = V_g(r_0)\, C_0(r_0). \quad (3)$$

The implicit assumption here is that what goes up must come down. That is, although V_g is an obvious downward velocity, it is equivalent to the original upward *production* velocity. The upshot of (3) is that, if we know dF/dr_0, we can estimate the spray concentration profile as a function of height from an equation like (1).

[9] Because (3) is not accurate for smaller droplets, the deposition velocity V_D [e.g., *Slinn and Slinn*, 1980; *Williams*, 1982; *Slinn*, 1983; *Fairall and Larsen*, 1984] is usually presumed to be better for relating droplet concentration and the spray generation function. Under the assumption that the near-surface spray is in equilibrium (again, that the average upward transport of droplets of radius r_0 is equal to their average downward deposition), the effective spray generation function at arbitrary height z, $dF/dr_0|_z$, can be related to the concentration at z of droplets with radius r_0 through the deposition velocity appropriate at height z, $V_D(z,r_0)$ [e.g., *Hoppel et al.*, 2002, 2005]:

$$dF/dr_0\big|_z = V_D(z, r_0)\, C(z, r_0). \quad (4)$$

An equally important use of (4) is to infer the effective spray generation function at z from measurements of the spray concentration $C(z,r_0)$ and calculations of the deposition velocity at z [e.g., *Smith et al.*, 1993]. In turn, *Fairall and Larsen* [1984], *Andreas* [2002], and *Hoppel et al.* [2002] show how to obtain dF/dr_0 from $dF/dr_0|_z$ and calculations of the deposition velocity.

[10] Theoretical formulations for the deposition velocity have not been validated, however, because only one of the three unknowns in (4) is observable at sea, the droplet concentration $C(z,r_0)$. Therefore, we here try to validate predictions for the deposition velocity indirectly. The literature contains several adequate sets of observations of droplet concentration $C(z,r_0)$ measured within one significant wave height of the sea surface. When *Andreas* [2002] reviewed spray generation, he identified several spray generation functions that seem most reliable. By combining a prediction of the spray generation function, dF/dr_0, with near-surface observations of droplet concentration, which we denote as $C_0(r_0)$, we can test the validity of relations like (3) and (4) in the form

$$\frac{dF/dr_0}{C_0(r_0)} = V_{eff}(r_0). \quad (5)$$

[11] Here, $V_{eff}(r_0)$ is the effective droplet velocity that links the near-surface droplet concentration with the effective upward surface flux of droplets. In effect, we interpret V_{eff} as a spray production velocity. One candidate expression for V_{eff}, of course, is the deposition velocity; but we also consider three other possible velocity scales. Namely, the local wind speed is an obvious scale that should be related to spray production; the friction velocity u_* is also. Last, *Blanchard* [1963] measured the velocity with which jet droplets are ejected from bursting bubbles; this ejection velocity is another candidate.

[12] In the next sections, we explain our choice for the best current spray generation function, review observations of the near-surface spray droplet concentration, and elaborate on each of these four candidate velocity scales. The observations that we consider span droplets with radii from 5 to 300 μm. Throughout this radius range, the theoretical deposition velocity is less than the implied V_{eff}: That is, we do not confirm (4), a result that calls into question all spray generation functions based on this premise. A velocity scale related to u_* has a range of droplet radii where it agrees with the implied V_{eff}, but we conclude that this is fortuitous agreement. On the other hand, both the jet droplet ejection velocity and the wind speed computed at the crest of the waves agree with V_{eff} over a wide range of radii: from 20 to 300 μm. Both are useful scales for the spray production velocity in our data set, but we suspect that the ejection velocity is not generally appropriate because is says nothing about spume production.

2. Spray Generation Function

[13] Although the spray generation function dF/dr_0 is still an issue of debate, especially for droplet radii larger than 10–20 μm, *Andreas* [2002] identified two functions, spanning radii from 0.5 to 500 μm, that seem to have proper magnitude and wind speed dependence. The function from *Monahan et al.* [1986] covers droplets with radii r_0 from 0.5 to 20 μm, treats wind speeds up to 25 m s^{-1}, and has been repeatedly proven to be accurate for predicting the production of these smaller droplets [cf. *Gong*, 2003]. *Andreas* [2002], in turn, judged the function from *Fairall et al.* [1994] to be the best available for larger droplets. This function covers droplets with r_0 from 1.6 to 500 μm and also treats wind speeds up to 25 m s^{-1}. *Fairall et al.* [1994], *Andreas* [2004, 2010], and *Andreas et al.* [2008] obtained reasonable predictions of various spray processes using the *Fairall et al.* function.

[14] Because we wanted for this study a single spray generation function that reliably spans r_0 values from 0.5 to 500 μm [*Jones and Andreas*, 2009], we merged the *Monahan et al.* [1986] and *Fairall et al.* [1994] functions in the radius range 1.5–2.0 μm. Joining these functions was straightforward because they have the same wind speed dependence. *Monahan et al.* [1986] give the equations that we use for their portion of dF/dr_0; we use only their formulation for the spray produced by bursting bubbles. *Andreas* [2002] gives the equations for the *Fairall et al.* function, which were not specified in the original paper.

[15] Both *Monahan et al.* [1986] and *Fairall et al.* [1994], however, predict dF/dr_{80}, where r_{80} denotes the droplet radius in equilibrium at a relative humidity of 80%. We convert this function to dF/dr_0 from [*Andreas*, 1992, 2002]

$$\frac{dF}{dr_0} = \frac{dr_{80}}{dr_0}\,\frac{dF}{dr_{80}}, \quad (6)$$

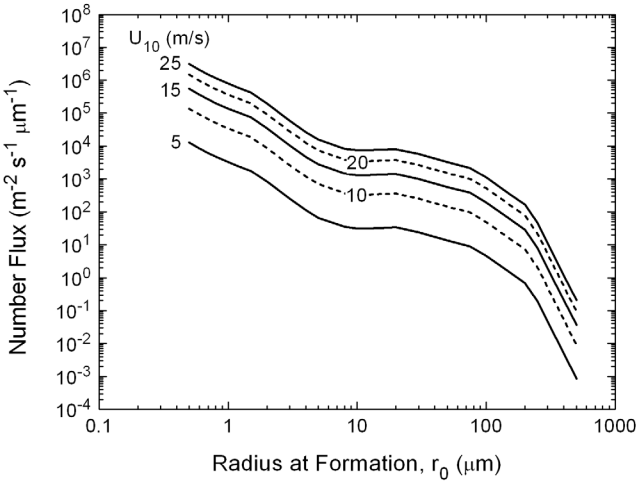

Figure 1. The spray generation function dF/dr_0, where r_0 is the droplet radius at formation. This function merges the small-radius function from *Monahan et al.* [1986] with the large-radius function from *Fairall et al.* [1994] in the r_0 interval 1.5–2.0 μm.

where

$$\frac{dr_{80}}{dr_0} = 0.506\, r_0^{-0.024}. \quad (7)$$

Equation (7) is accurate for typical ocean salinities of 30–36 psu, and here r_0 must be expressed in micrometers.

[16] Figure 1 shows the dF/dr_0 curves that we obtained by joining the *Monahan et al.* [1986] and *Fairall et al.* [1994] functions. Notice, for radii ranging between 0.5 and 500 μm, the number of droplets produced spans seven orders of magnitude. In line with the analyses by *Andreas* [2002] and *Lewis and Schwartz* [2004, chap. 5], we presume that the uncertainty in this dF/dr_0 is a factor of 4–5. That is, the true function could be a multiplicative factor of 4–5 times larger or 0.20–0.25 times smaller.

3. Near-Surface Spray Concentration Data

[17] To implement (5), we require measurements of the near-surface spray concentration over the ocean, $C_0(r_0)$. Although many measurements of spray droplet concentration in the marine boundary layer exist [e.g., *Lewis and Schwartz*, 2004, Figure 22], surprisingly few have been made within one significant wave height of the sea surface where we can presume that the measured C(z,r) is approximately $C_0(r_0)$, where r is the observed droplet radius.

[18] We have located 13 acceptable data sets in the literature. Table 1 summarizes the conditions under which these data were collected. Eleven of the 13 sets of observations were made within one significant wave height of the sea surface. For *Monahan*'s [1968] observations in Buzzard's Bay, we assume the surface salinity was 30 psu; for all the other observations, we assume the salinity was 34–35 psu.

[19] Besides wind speed, Table 1 lists surface temperature, air temperature, relative humidity, and significant wave height ($H_{1/3}$). Later in our analysis, we use these forcing variables to compute the friction velocity, u_*, and the wind speed profile from the bulk air-sea flux algorithm that *Andreas et al.* [2008] developed. *de Leeuw* [1986a, 1986b, 1987] reported $H_{1/3}$, but the other sources did not. When $H_{1/3}$ is unavailable, the Andreas et al. routine computes it from *Andreas and Wang*'s [2007] algorithm. Later, $H_{1/3}$ will be a key height scale in our analysis.

[20] Figure 2 shows the droplet concentration measurements that we gleaned from the sources in Table 1. In general in this plot, the concentrations spread out according to wind speed: Higher wind speeds produce higher concentrations.

Table 1. Sources of the Near-Surface Spray Concentrations Used Here[a]

Source	Height (m)	U (m s^{-1})	RH (%)	T_s (C)	T_a (C)	$H_{1/3}$ (m)	u_* (m s^{-1})	Location
de Leeuw [1986a]								
Figure 2	≤2.0	5.5	70	(10)	(9)	0.5	0.197	North Atlantic on
Figure 3	≤1.0	7	61	(10)	(9)	1.5	0.258	Station Lima
Figure 4	≤2.0	13	68	(10)	(9)	2.5	0.534	(57°N, 20°W)
de Leeuw [1986b]								
Figure 2	≤2.0	8.5	64	(10)	(9)	1.5	0.321	Same
de Leeuw [1987]								
Figure 1	≤0.75	8.9	75	(11)	(10)	0.95	0.339	North Sea on
Figure 2	≤1.0	12.4	80	(11)	(10)	1.71	0.504	Meetpost Noordwijk
de Leeuw [1990]								
Figure 5	<1.0	7.7	87	11.0	10.4	(1.0)	0.283	Same
Figure 6	<1.0	12	61	13.7	11.7	(1.6)	0.489	
Figure 7	≤2.0	14	80	13.5	10.4	(1.9)	0.592	
Monahan [1968]								
Figure 2	0.13	11	(80)	(26)	(25)	(2.75)	0.438	Off Aruba
Figure 3	0.13	16	(80)	(12)	(11)	(1.18)	0.689	Buzzard's Bay
Preobrazhenskii [1973]								
Figure 2a	1.5–2.0	7–12	(80)	(10)	(9)	(2.0)	0.379	North Atlantic
Figure 2b	1.5–2.0	15–25	(80)	(10)	(9)	(7.0)	0.967	

[a]U is the reported wind speed; for *Preobrazhenskii*'s [1973] two ranges, we used the midpoints 9.5 and 20 m s^{-1} for our calculations. de Leeuw always reported the relative humidity, RH, and usually reported the significant wave height, $H_{1/3}$. "Height" gives the height of the spray concentration measurements. All of de Leeuw's data are reported as profiles; for $C_0(r_0)$, we used the largest near-surface concentration in the profile. This was not always the values observed at the lowest level. T_s and T_a are the surface and air temperatures, respectively. Temperature and humidity values in parentheses are inferred from climatology. *de Leeuw* [1990] did not report air or surface temperature; the values here come from *DeCosmo* [1991]. The $H_{1/3}$ values in parentheses come from *Andreas and Wang*'s [2007] algorithm, which computes $H_{1/3}$ from wind speed and water depth. All friction velocities, u_*, were computed from the other conditions using the *Andreas et al.* [2008] bulk flux algorithm.

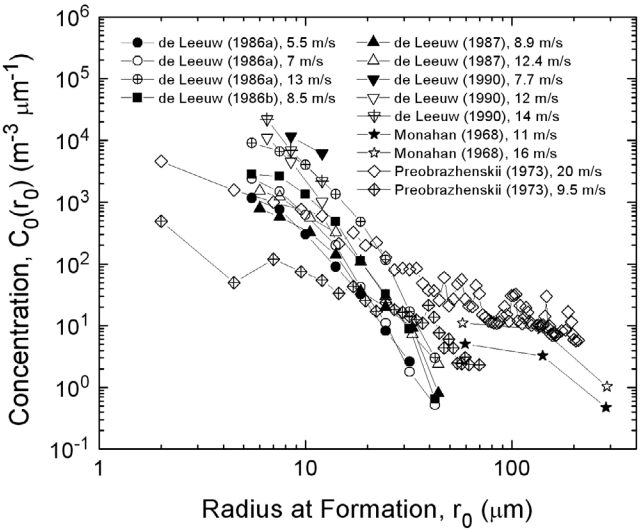

Figure 2. Near-surface spray concentrations reported by the sources in Table 1.

The two data points from *de Leeuw* [1990], collected in winds of 7.7 m s^{-1}, are obvious outliers. The data from *Preobrazhenskii* [1973] (both sets) for radii less than about 20 μm seem biased low. We suspect that his inertial collection system was much less than 100% efficient in collecting these smaller droplets; they are, thus, under sampled. Preobrazhenskii's larger droplets agree well with *Monahan*'s [1968] observations, however.

[21] An ever-present issue in studying the marine aerosol is standardizing the reporting of droplet size [e.g., *Andreas et al.*, 2001; *Andreas*, 2002]. All of the data sources in Table 1 seem to report the observed droplet size. That is, none converted the observed droplet radius r to a common standard like r_0, r_{80}, or r_{eq}, the droplet radius in equilibrium at the ambient humidity. We therefore had to impose a sizing convention on the data ourselves.

[22] *Andreas* [1992] [see also *Andreas and DeCosmo*, 1999] defined several time scales to use for characterizing droplet evolution. The ones pertinent for this discussion are the residence time, τ_f, and the e-folding time for radius evolution, τ_r.

[23] The radius at any time t, r(t), of droplets formed with initial radius r_0 (at t = 0) follows an exponential evolution curve:

$$\frac{r(t) - r_{eq}}{r_0 - r_{eq}} = \exp(-t/\tau_r). \quad (8)$$

Here, τ_r is the e-folding time of the radius evolution, and r_{eq} is the equilibrium radius. r_{eq} depends on ambient conditions and the salinity of the ocean surface; clearly, r_{eq} obtains when $t \gg \tau_r$. *Andreas* [2005a] gives the algorithms that we use for computing r_{eq} and τ_r.

[24] The second time scale approximates the residence time of a droplet. Most spray droplets form near wave crests from bubbles bursting in whitecaps and as spume torn from the crests. *Andreas* [1992] therefore suggested estimating the residence time as

$$\tau_f = \frac{H_{1/3}/2}{V_g(r_0)}. \quad (9)$$

Here, V_g is again the terminal fall speed of a droplet with radius r_0 (always taken as positive), and $H_{1/3}$ is the significant wave height. Equation (9) simply says that a droplet is in the air, roughly, for as long as it takes to fall from its formation height to mean sea level. When the data source did not give $H_{1/3}$, we computed it from *Andreas and Wang*'s [2007] algorithm in the course of running the bulk flux algorithm given by *Andreas et al.* [2008].

[25] To help us decide how to interpret the droplet sizes reported in the sources in Table 1, we made plots to compare τ_r and τ_f. Figure 3 is one such example. For droplet sizes reported by *de Leeuw* [1986b], we computed τ_r and τ_f for two mutually exclusive assumptions: that the reported droplet size was r_0 and that the reported size was r_{eq}. For the assumption that the reported size is r_0, (8) and (9) are immediately accurate. For the assumption that the reported size is r_{eq}, we first converted r_{eq} to its associated r_0 using *Lewis and Schwartz*'s [2006] relation and then found τ_r and τ_f for droplets of this size.

[26] In Figure 3, the τ_r and τ_f curves cross at r_0 = 26 μm. Smaller droplets remain suspended long enough to be near r_{eq} when they fall back into the sea. Larger droplets, in contrast, are closer to r_0 when they return to the sea. We therefore interpret Figure 3 to mean that the assumption that the reported droplet size is r_{eq} is not true for droplets to the right of this crossover: Most simply did not have enough time to reach their equilibrium radius.

[27] In all other such plots that we made, the τ_r–τ_f crossover was always in the vicinity of r_0 = 20 μm. The actual position depends on wind speed (through its influence on $H_{1/3}$) and relative humidity. We see in Figure 2 that many of the droplets in our data set are larger than 20 μm and, thus, must have been close to their initial radius, r_0, when observed. The smaller droplets in our data set were probably closer to r_{eq} when observed. We will keep this distinction in

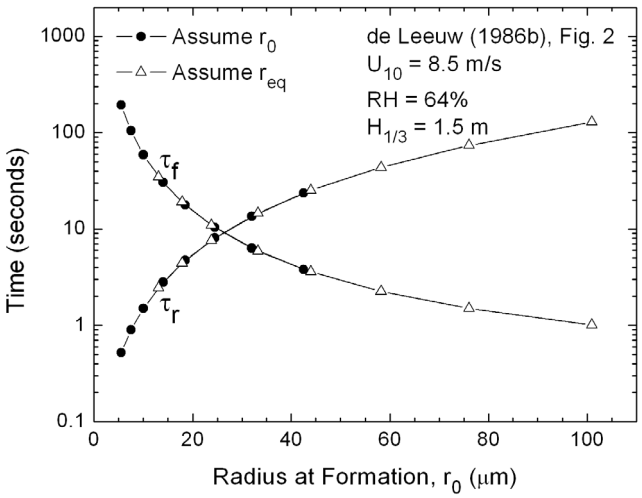

Figure 3. The time scales τ_f and τ_r for the droplet sizes observed by *de Leeuw* [1986b, Figure 2]. de Leeuw reported the 10 m wind speed (U_{10}), the relative humidity (RH), and the significant wave height ($H_{1/3}$). The plot shows τ_f and τ_r computed for two assumptions: the observed droplet size was the radius at formation, r_0, and the observed size was the equilibrium radius, r_{eq}.

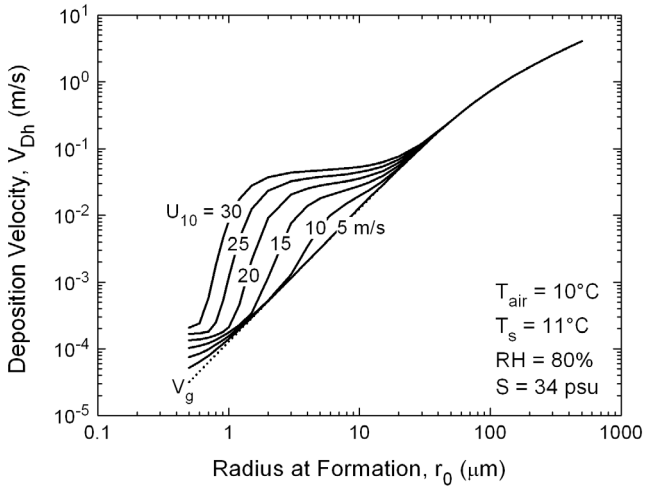

Figure 4. Calculations of the deposition velocity V_{Dh} at height $h = H_{1/3}/2$ for values of the 10 m wind speed, U_{10}, between 5 and 30 m s^{-1}. Air temperature was assumed to be 10°C; surface temperature, 11°C; relative humidity, 80%; surface salinity, 34 psu; and barometric pressure, 1000 mbar. The dotted line shows the terminal fall speed, V_g, which is the same as V_{Dh} for large radii.

mind when interpreting our results but will base all subsequent calculations on the assumption that the reported droplet radius is r_0.

4. Spray Production Velocities

4.1. Deposition Velocity

[28] Most modern treatments of the deposition velocity build on models by *Slinn et al.* [1978], *Slinn and Slinn* [1980], and *Slinn* [1983] for dry deposition to a water surface [cf. *Williams*, 1982; *Fairall and Larsen*, 1984]. These deposition models are presumed to be useful for connecting the near-surface droplet concentration to the rate of spray generation under the assumption that the spray concentration is in equilibrium: what goes up must come down [e.g., *Fairall and Larsen*, 1984; *Smith et al.*, 1993].

[29] In Appendix A, we derive the expression for the deposition velocity that we use here. It is

$$V_{Dh} = \frac{V_g + V_a}{1 + \frac{V_a}{V_g}(1 - f_{\delta h})}. \tag{10}$$

Here, V_g is still the terminal fall velocity of droplets with radius r_0, V_a is another velocity that characterizes the rate at which droplets of r_0 cross the molecular sublayer on the air side of the sea surface (see (A30)). This sublayer has thickness

$$\delta = 25\frac{\nu}{u_*}, \tag{11}$$

where ν is the kinematic viscosity of the air. Last, in (10),

$$f_{\delta h} = \exp\left[-\frac{V_g}{k\,u_*}\ln\left(\frac{h}{\delta}\right)\right] = \left(\frac{h}{\delta}\right)^{-V_g/ku_*} \tag{12}$$

is related to the vertical profile of droplets with radius r_0 (cf. equation (1)).

[30] In our conceptual picture [*Fairall et al.*, 2009], the spray concentration profile $C(z,r_0)$ is constant from the sea surface up to height h. The effective spray generation function, $dF/dr_0|_z$, is likewise assumed to be constant for $0 \le z \le h$. Hence, we interpret $dF/dr_0|_{z=h}$ as the dF/dr_0 values plotted in Figure 1 and $C(h,r_0)$ as the C_0 values plotted in Figure 2. The deposition velocity (10) then provides the equality

$$dF/dr_0 = V_{Dh}\, C_0. \tag{13}$$

For h in (10), (12) and (13), we take $H_{1/3}/2$, the significant wave amplitude [cf. *Iida et al.*, 1992], which we have already used as the key height for estimating residence time, (9).

[31] *de Leeuw*'s [1986a, 1986b, 1987, 1990] measured droplet concentration profiles are the basis for this conceptual model that consists of three layers: a molecular sublayer, a well-mixed middle layer that extends up to the wave crests, and the atmospheric surface layer. de Leeuw's data suggest that droplet concentration does not change much with height below the crests of the waves but typically decreases with height above the wave crests.

[32] *Hoppel et al.* [2002, 2005] also recently derived expressions for the deposition velocity. Our result differs from the one of *Hoppel et al.* [2002] because they consider no molecular sublayer and assume that the concentration and the spray generation at some reference height δ are essentially the surface values. (Notice, their δ is comparable in magnitude to our h.)

[33] The results of *Hoppel et al.* [2002, equation (34′)] and *Hoppel et al.* [2005, equation (37)] for "no surface source" have the same form as our (10) although the details of V_a differ. In Appendix A, though, we explain that (10) applies both with and without a surface source of spray droplets. *Hoppel et al.* [2005], on the other hand, derive a different expression for the deposition velocity in the presence of a surface source of spray.

[34] Figure 4 shows the deposition velocity for several values of the 10 m wind speed, U_{10}. We use the *Andreas et al.* [2008] bulk air-sea flux algorithm and the conditions given in Figure 4 to compute quantities necessary for calculating V_{Dh} from (10), like u_* and $H_{1/3}$.

[35] Figure 4 has features similar to other plots of deposition velocity in the literature [e.g., *Giorgi*, 1986; *Smith et al.*, 1993; *Hoppel et al.*, 2002]. The dashed line shows V_g, the terminal fall speed. For droplets larger than about 30 μm, the deposition velocity is essentially V_g. For smaller droplets, V_{Dh} deviates more and more from V_g as wind speed increases. This enhanced deposition velocity is a consequence of our including Brownian diffusion through the molecular sublayer and turbulence-induced droplet inertia in the formulation for V_{Dh}. Turbulent mixing, which increases with increasing wind speed, allows droplets to cross the molecular sublayer more rapidly than gravitational settling does. Of course, processes and parameterizations for the molecular sublayer are the least certain in this analysis [e.g., *Slinn*, 1983].

[36] Equation (12) is part of the traditional solution for the droplet concentration profile [e.g., *Hoppel et al.*, 2005]. As

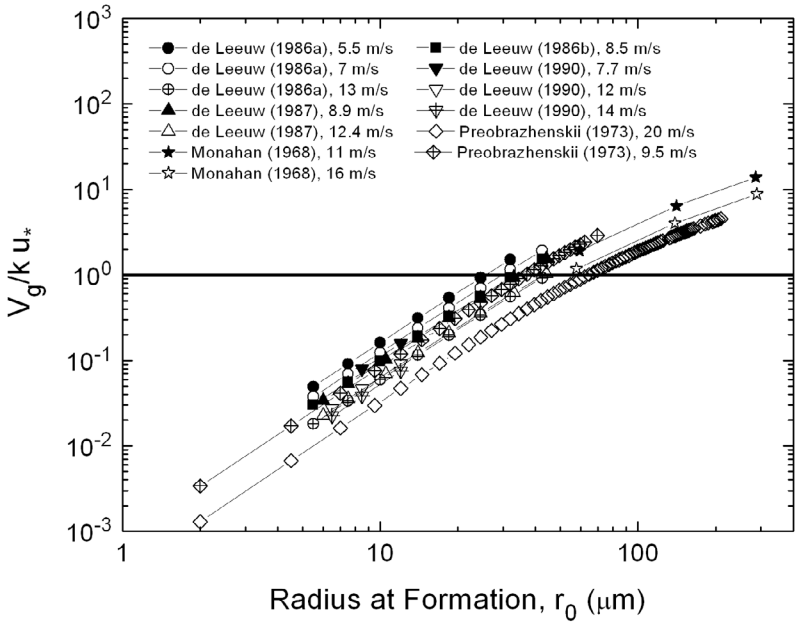

Figure 5. Calculations of V_g /k u_* as a function of the radius at formation, r_0, for each of the data sets listed in Table 1. The line at V_g /k u_* = 1 traditionally separates regimes in which gravitational settling dominates turbulent suspension (above the line) and vice versa (below the line).

such, the V_g/ku_* term is typically taken as an indicator of whether a droplet of radius r_0 will fall back into the ocean locally or remain suspended [e.g., *Wu*, 1982]. When $V_g/ku_* > 1$, gravitational settling dominates turbulent suspension. When $V_g/ku_* < 1$, turbulent suspension dominates, and vertical concentration gradients are small.

[37] Figure 5 shows our calculations of V_g/ku_* for each set of droplet radii and environmental conditions listed in Table 1. Depending on wind speed, the traces in Figure 5 cross the $V_g/ku_* = 1$ threshold for r_0 values between 25 and 66 μm. Data collected in lower winds cross to $V_g/ku_* > 1$ at smaller radii than do data collected in higher winds. These results are supplementary to the τ_f–τ_r analysis in Figure 3 and highlight three regimes in our data set. For $r_0 > 66$ μm, all droplets would return quickly to the surface and would have had radii near r_0 when they were observed. For $r_0 < 26$ μm, droplets fall more slowly and were probably closer to a radius of r_{eq} when they were observed. For $26 \le r_0 \le 66$ μm, the observed droplets were in transition between a radius of r_0 and a radius of r_{eq}. Of course, we can apply specific limits to every trace in Figure 5, but these general guidelines will focus our subsequent discussion.

4.2. Wind Speed at the Wave Crest

[38] Anyone who has watched the sea in high winds has seen spray droplets forming near the wave crests and being swept upward by the wind. These droplets have an obvious vertical component to their velocity that should, intuitively, be related to the local wind speed and to the steepness of the waves [cf. *Fairall et al.*, 2009]. In other words, if the near-surface wind is traveling faster than the waves, it follows streamlines dictated by the local water surface and, thus, will have an upward component when it reaches the wave crests. This local wind drags spray droplets away from the surface.

[39] We can predict the magnitude of the upward wind component from the wave steepness S. A traditional definition of wave steepness is wave height over wavelength [e.g., *Kinsman*, 1965, p. 11; *Tucker and Pitt*, 2001, p. 85f.]. Therefore, if we suppose again that a representative height of the wave crests above mean sea level is $A_{1/3} = H_{1/3}/2$ and denote the mean wind speed at this height as $U_{A_{1/3}}$, geometry implies that the vertical component of the wind at the wave crest is

$$W_{cr} = U_{A_{1/3}} S. \tag{14}$$

[40] When waves are breaking and creating spray, however, a wave steepness based on the significant wave height and the wavelength of the dominant waves is not a good model for the sea surface slope on the windward face of breaking waves. *Massel* [2007, chap. 4] discusses the difference between this "global" steepness, which is in the range of 0.01–0.1 [*Kinsman*, 1965, p. 11; *Tucker and Pitt*, 2001, p. 86; *Massel*, 2007, p. 116ff.] and the local steepness near the crests of breaking waves. This local steepness is found to have values between 0.2 and 1 [*Massel*, 2007, Tables 4.1, 4.7, 4.8, and 4.9]. Consequently, from (14), the vertical velocity component carrying spray up from the crests of breaking waves can have a magnitude that is of the same order as $U_{A_{1/3}}$.

[41] *Mueller and Veron*'s [2009a] numerical modeling supports this conceptual picture. The ratio of their modeled near-surface vertical velocity over the windward face of waves to the local horizontal velocity approximately equals the local wave slope.

[42] Because our data sets do not include enough wave details to let us calculate S, we simply use $U_{A_{1/3}}$ as an

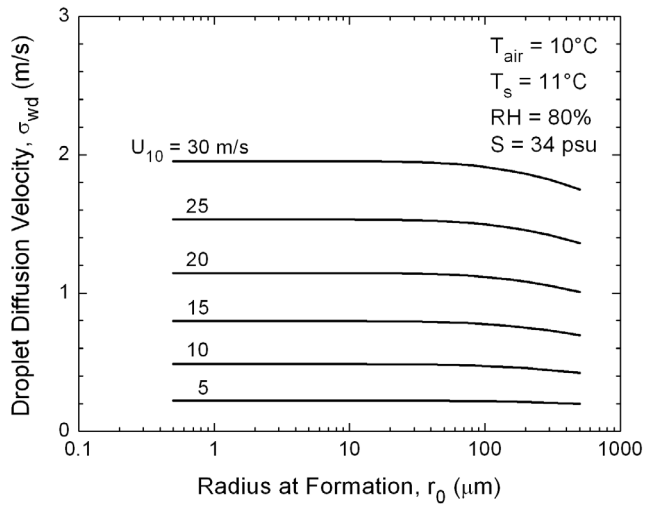

Figure 6. Calculations from (21) of the standard deviation in droplet diffusion velocity, σ_{wd}. Conditions are as in Figure 4.

estimate of W_{cr}. We calculate $U_{A_{1/3}}$ from the standard surface-layer profile relation [e.g., *Garratt*, 1992, p. 53]:

$$U_{A_{1/3}} = \frac{u_*}{k}\left[\ln\left(A_{1/3}/z_0\right) - \psi_m\left(A_{1/3}/L\right)\right]. \tag{15}$$

In this, k is, again, the von Kármán constant; z_0 is the roughness length for wind speed; L is the Obukhov length, a stratification parameter; and ψ_m is a known function of stratification. The bulk flux algorithm [i.e., *Andreas et al.*, 2008] that is the "front end" of all our subsequent computations provides u_*, z_0, L, and ψ_m from the conditions listed in Table 1.

4.3. Turbulent Diffusion of Droplets

[43] Once created, droplets are carried up and down by turbulence. Because of their mass, spray droplets cannot follow the turbulence exactly, however. The Langevin equation is therefore often used recursively to model droplet trajectories in a turbulent flow [e.g., *Edson and Fairall*, 1994; *Pattison and Belcher*, 1999]. Since the vertical velocity component is responsible for carrying droplets away from the sea surface, we focus only on it:

$$w_d(t+\Delta t) = \left(1 - \frac{\Delta t}{\tau_{L,d}}\right) w_d(t) + \sigma_{wd}\left(\frac{2\Delta t}{\tau_{L,d}}\right)^{1/2} \xi. \tag{16}$$

Here, w_d is a droplet's instantaneous vertical velocity; t is the current time; Δt is the time step; $\tau_{L,d}$ is the droplet's Lagrangian integral scale, a measure of the droplet's memory of past motions; σ_{wd} is the standard deviation in the vertical velocity of the droplet; and ξ is a random number chosen from a normal distribution with zero mean and unit variance.

[44] We are not going to do any droplet trajectory modeling but present (16) as our motivation for focusing on σ_{wd} as a third potential velocity scale for predicting spray production. This quantity usually takes a from like [e.g., *Meek and Jones*, 1973; *Edson and Fairall*, 1994; *Pattison and Belcher*, 1999]

$$\sigma_{wd} = \frac{\sigma_w}{(1+\chi)^{1/2}}. \tag{17}$$

In this, σ_w is the standard deviation in the vertical velocity of the fluid, which we take as [e.g., *Panofsky and Dutton*, 1984, p. 160; *Kaimal and Finnigan*, 1994, p. 16]

$$\sigma_w = 1.25\ u_* \tag{18}$$

in neutral stratification. We could add stratification effects to (18) following *Kaimal and Finnigan* [1994, p. 16], for instance; but that minor tuning is unwarranted at this stage of our investigation.

[45] The χ in (18) parameterizes how droplet inertia reduces σ_{wd} from σ_w. We write it as

$$\chi = \frac{V_g(r_0)}{g\ \tau_L}. \tag{19}$$

Here, χ is size-dependent because it includes the droplet's terminal fall speed, V_g. Also in (19), g is the acceleration of gravity; and τ_L is the Lagrangian integral scale of the turbulence [*Pattison and Belcher*, 1999],

$$\tau_L = \frac{0.4z}{u_*}. \tag{20}$$

In (20), we ultimately take the height z to be the significant wave amplitude, $A_{1/3}$.

[46] On combining (17)–(20), we obtain our prediction for a representative vertical diffusion velocity for spray droplets:

$$\sigma_{wd} = \frac{1.25u_*}{\left(1 + \frac{V_g u_*}{0.4 g A_{1/3}}\right)^{1/2}}. \tag{21}$$

Notice, small droplets (for which V_g is very small) follow the turbulent flow well. As droplet size (and, thus, V_g) gets large, σ_{wd} should become progressively less than $\sigma_w = 1.25u_*$.

[47] Figure 6 shows, however, that we are not considering droplets large enough for their inertia to decrease σ_{wd} by much. Furthermore, because in our algorithm $A_{1/3}$ goes roughly as the square of the wind speed, droplet mass has a diminishing effect on droplet motion as the wind speed increases.

4.4. Ejection Velocity

[48] When an air bubble in a whitecap rises to the surface and bursts, it creates many, many small "film" droplets from the bubble cap and six or seven [e.g., *Spiel*, 1994] larger "jet" droplets from the water jet formed at the base of the collapsing bubble cavity. In the laboratory, *Blanchard* [1963, Figure 12] measured the ejection velocity, V_{ej}, of the top jet droplet and related it to the diameter of the parent bubble. *Blanchard* [1963, Figure 9] also related the size of the top jet droplet to the diameter of the parent bubble. We combined the results of these two figures into a look-up table that gives the ejection velocity as a function of initial droplet radius. Figure 7 shows the upward velocity with which the top jet droplet is ejected, V_{ej}.

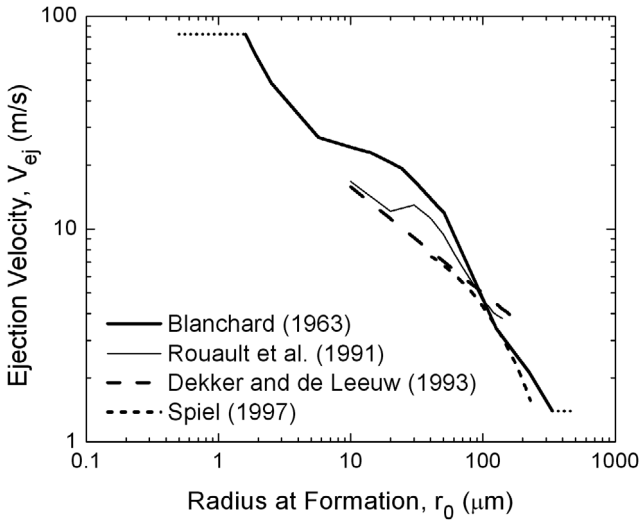

Figure 7. Estimates of the ejection velocity, V_{ej}, of the top jet droplet inferred from laboratory measurements by *Blanchard* [1963, Figures 9 and 12]. The solid curve is the range of Blanchard's data. The dotted lines are our extrapolations so we can span droplet sizes from 0.5 to 500 μm. For comparison, we also show estimates from *Rouault et al.* [1991] and *Dekker and de Leeuw* [1993] and *Spiel*'s [1997] laboratory results.

[49] *Rouault et al.* [1991] used a numerical model to calculate backward to the implied ejection velocity from maximum droplet ejection heights reported by *Blanchard* [1963]. *Dekker and de Leeuw* [1993] constructed a physics-based model of spray production and, thus, necessarily also had to predict V_{ej}. Figure 7 also shows ejection velocities from these two groups. Although neither set of estimates spans the radius range that *Blanchard*'s [1963] data does, the three sets agree well in the radius region that they share.

[50] *Spiel* [1995, 1997] made laboratory measurements of ejection velocities of the first few jet droplets, but the smallest droplets he treated were more than ten times larger than *Blanchard*'s [1963] smallest droplets. Spiel also found that ejection velocities of lower droplets in the jet set were smaller than for the top droplet. Figure 7 shows that, in the radius region where their measurements overlap, Spiel's and Blanchard's ejection velocities for the top jet droplet are comparable.

[51] Although V_{ej} is associated specifically with bursting bubbles and, in the ocean, bursting bubbles cluster in whitecaps, it is not illogical for us to use V_{ej} as a candidate for the spray production velocity. Remember, we interpret dF/dr_0 and $C_0(r_0)$ in (5) as areal averages despite the heterogeneity in spray production. Likewise, we interpret V_{ej} as an areal average (with the values shown in Figure 7), in exact analogy with dF/dr_0.

[52] Furthermore, though V_{ej} admittedly should explain only the production velocity of jet droplets, we consider it as our fourth and final candidate velocity because the production of jet droplets presumably dominates dF/dr_0 for intermediate r_0 values.

5. Effective Production Velocity

[53] Using (5), we calculated the effective spray production velocity V_{eff} implied by dF/dr_0 and the concentration data in Figure 2. Figure 8 is a plot of these velocities.

[54] Again, the two data points from *de Leeuw* [1990] for a wind speed of 7.7 m s^{-1} are outliers on this plot. *Preobrazhenskii*'s [1973] data for droplets with radii smaller than 20 μm produce large velocities because, we believe, his sampling was inefficient in catching these small droplets; C_0

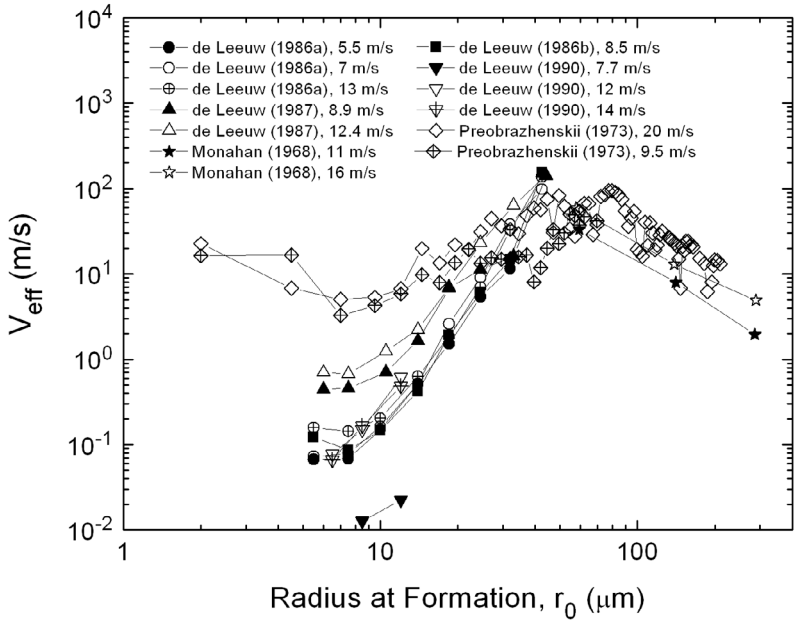

Figure 8. The effective spray production velocity computed from (5), the concentration data displayed in Figure 2, and the joint *Monahan et al.* [1986] and *Fairall et al.* [1994] spray generation function (i.e., Figure 1).

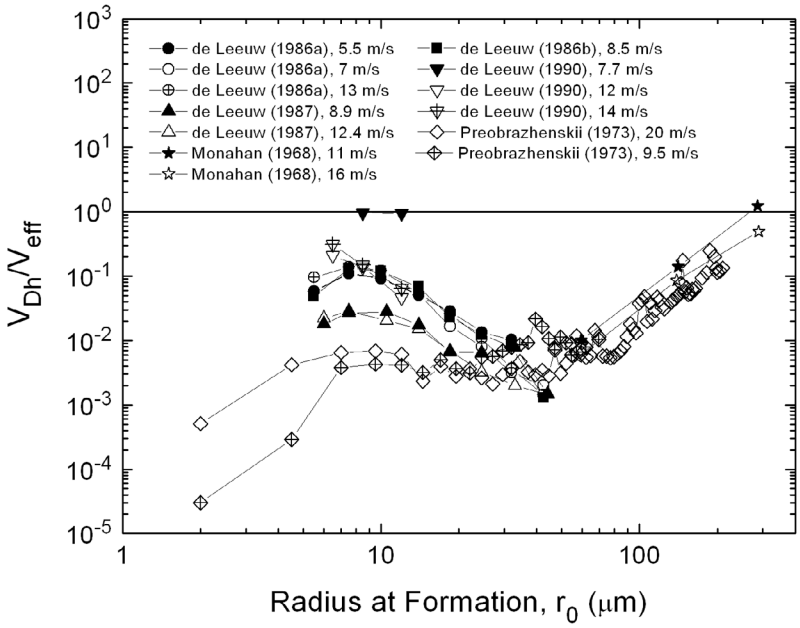

Figure 9. The ratio of computed deposition velocity, V_{Dh}, to effective spray production velocity, V_{eff} (see Figure 8), as a function of initial droplet radius, r_0.

in (5) is thus too small, and V_{eff} is too large. The other data in Figure 8 are quite consistent: V_{eff} has a range of only about one order of magnitude for any of the observed radii.

[55] To see whether any of our candidate production velocities, V_{can}, can predict the effective production velocity, we show in Figures 9–12 the velocity ratios V_{can}/V_{eff}, where V_{can} is V_{Dh}, $U_{A_{1/3}}$, σ_{wd}, and V_{ej}, respectively. If V_{can} is a good predictor of V_{eff}, the ratio will be near one; but any ratio between 0.2 and 5 indicates good agreement because of the uncertainty in dF/dr_0.

[56] Figure 9 suggests that the deposition velocity is a poor predictor of spray production. Except for a few points with $r_0 < 10$ μm, for *de Leeuw*'s [1990] two suspect points, and for *Monahan*'s [1968] two largest droplet sizes, V_{Dh} is typically an order of magnitude or more smaller than V_{eff}. Although uncertainty still exists in some aspects of modeling V_{Dh}, most computed values in the literature are comparable to ours. That is, our computed V_{Dh} values are unlikely to be 10–100 times too small.

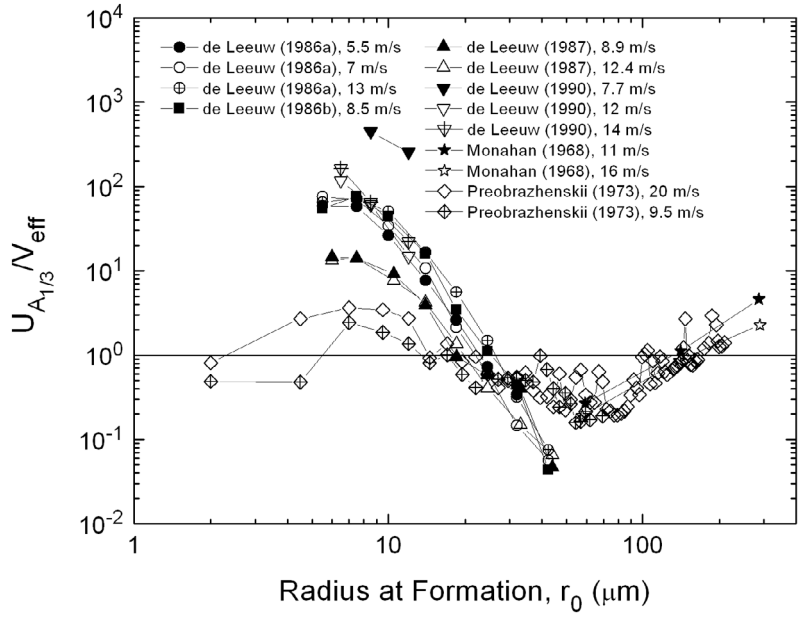

Figure 10. As in Figure 9, except this shows the ratio of mean wind speed at the wave crests, $U_{A_{1/3}}$, to V_{eff}.

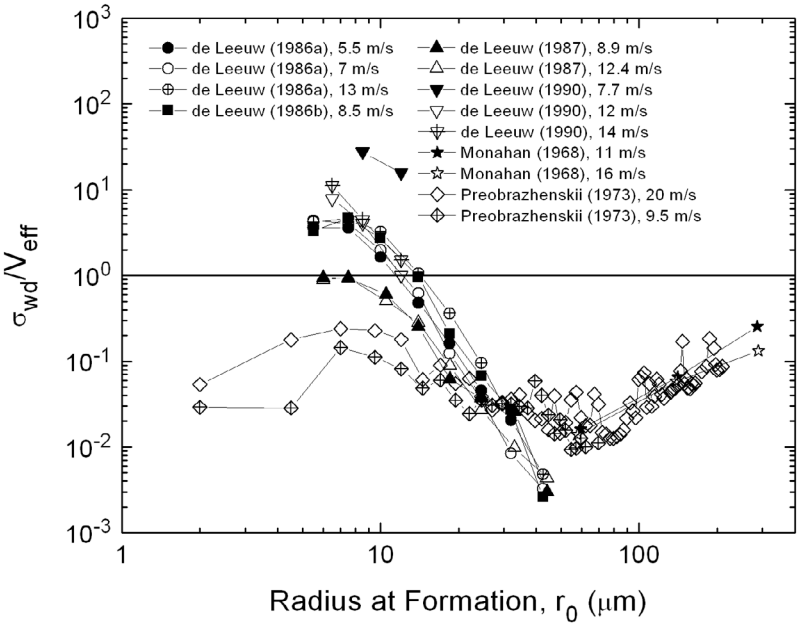

Figure 11. As in Figure 9, except this shows the ratio of the standard deviation in vertical droplet velocity, σ_{wd}, to V_{eff}.

[57] Using V_{Dh} to predict spray generation presumes equilibrium between upgoing and depositing droplets. This assumption of equilibrium should get progressively better as droplet size increases but, intuitively, should be appropriate for all droplets for which $V_g/ku_* > 1$. Remember, V_g/ku_* is larger than one for all data in our set for which $r_0 > 66$ μm (Figure 5). The boundary layer mixing time to reach steady state [*Fairall and Larsen*, 1984] suggests a similar conclusion. For droplets of radius greater than about 66 μm, the mixing time to reach steady state is about one hour; but that mixing time approaches a day for smaller droplets.

[58] In Figure 9, however, droplets near this limit of 66 μm are still near the minimum in V_{Dh}/V_{eff}. As droplet radius increases above this critical radius, V_{Dh}/V_{eff} does climb toward one. Although we do not have enough data for large droplets to confirm this result, we speculate, on the basis of Figure 9, that V_{Dh} becomes comparable to V_{eff} only for droplets with r_0 larger than 200 μm. Notice, too, from

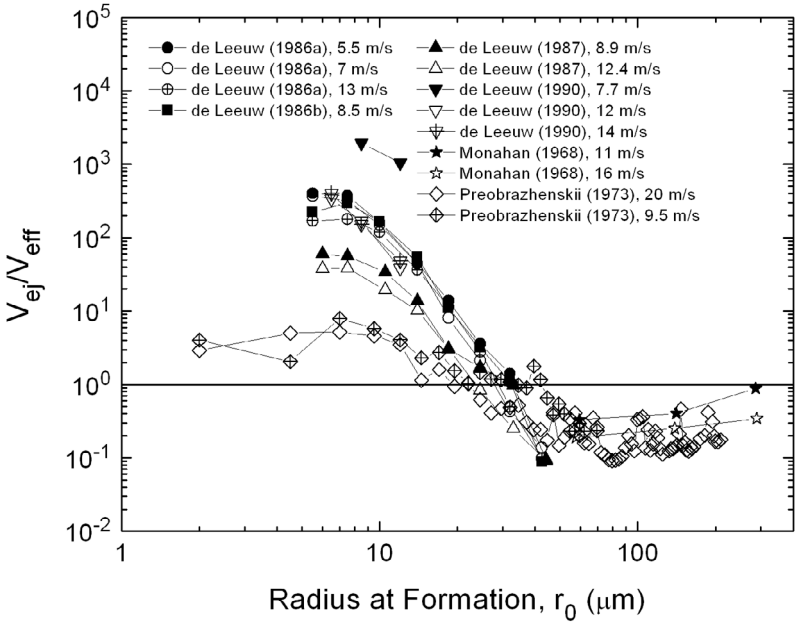

Figure 12. As in Figure 9, except this shows the ratio of the ejection velocity, V_{ej}, based on *Blanchard*'s [1963] observations, to V_{eff}.

Figure 4, that V_{Dh} is essentially V_g for all droplets with $r_0 > 30$ μm.

[59] Because V_{Dh} is a removal velocity, to estimate the production velocity from it, we should formally add the removal velocity at the top of the boundary layer [e.g., *Fairall and Larsen*, 1984; *Hoppel et al.*, 2002]. This latter velocity is the entrainment velocity at the top of a growing boundary layer, W_e. Consequently, the candidate effective velocity that is related to V_{Dh} should be $V_{Dh} + W_e$.

[60] Because W_e is on the order of 1 cm s^{-1} [e.g., *Fairall and Larsen*, 1984; *Stull*, 1988, pp. 478 and 483], adding it to V_{Dh} could have a big effect for droplets with radii of about 20 μm and smaller (see Figure 4). In our data set, however (for which radii generally are 5 μm and larger), $V_{Dh} + W_e$ is approximately twice as large as just V_{Dh} for droplets up to 10 μm. For larger droplets, adding W_e to V_{Dh} would have a negligible effect. As a result, in Figure 9, points for which r_0 is 10 μm or less would move a bit closer to one (by approximately 0.1); larger droplets would move negligibly upward. Hence, our results are largely unaffected by our ignoring W_e.

[61] Figure 10 shows the ratio of mean wind speed at the wave crests, $U_{A_{1/3}}$, to the calculated effective spray production velocity. For small droplets, $U_{A_{1/3}}$ is much larger than V_{eff}; but for droplets with radii r_0 from 20 to 300 μm, $U_{A_{1/3}}/V_{eff}$ is close to one. It appears that, for these larger droplets, spray production is closely associated with the local wind speed. Or, at least, the local wind speed is largely responsible for transporting droplets formed near the water surface to heights where they can be observed. Of course, the target $U_{1/3}/V_{eff} = 1$ relies on our assumption that the local steepness of breaking waves is near one.

[62] Figure 11 shows the ratio σ_{wd}/V_{eff}, where σ_{wd} is the calculated standard deviation in vertical droplet velocity. From (21) and Figure 6, we saw that this velocity is basically $1.25u_*$. For larger droplets (radii of 20 μm and larger), σ_{wd} is too small to explain droplet production. But for the smallest droplets in our data set, σ_{wd} is within a factor of five of our calculated production velocity. In section 6, we will discuss whether this agreement between σ_{wd} and V_{eff} for these small droplets reflects appropriate physics or is just coincidence.

[63] Finally, Figure 12 shows our results for V_{ej}/V_{eff}, where V_{ej}, from *Blanchard*'s [1963] laboratory measurements, is an upper bound on the ejection velocity of jet droplets [cf. *Spiel*, 1995, 1997]. For $r_0 > 20$ μm, V_{ej} is close to or somewhat less than V_{eff}. Moreover, for $r_0 > 30$ μm, V_{ej}/V_{eff} is almost independent of radius. This is the longest range for which V_{can} has the same radius dependence as V_{eff} in any of our plots of candidate production velocity (i.e., Figures 9–12). For droplets smaller than 20 μm, V_{ej} is much larger than V_{eff}.

[64] Spume droplets (spray droplets with $r_0 \geq 20$ μm [*Andreas*, 2002] that are produced when the wind tears them from the wave crests) do not begin forming until the wind reaches a threshold speed. This threshold speed is in the range 8–11 m s^{-1} [*Monahan et al.*, 1983; *Andreas et al.*, 1995] and corresponds well with the transition to Beaufort force 5, which includes in its definition "chance of some spray" (meaning spume).

[65] Some of our droplet concentration data were collected in wind speeds below this spume threshold, but most come from this range or in winds above it. Indeed, for the radius range in Figure 12 where we find V_{ej}/V_{eff} to be constant (that is, for $r_0 > 30$ μm), only one point from *de Leeuw* [1986a], for which the wind speed 7 m s^{-1} is below the spume threshold, is within this radius range. All other concentration observations should include some spume droplets. Because V_{ej} is explicitly the production velocity of jet droplets, the behavior of V_{ej}/V_{eff} in Figure 12 is thus puzzling. We can only speculate that, for the wind speeds represented in our data set, jet droplets rather than spume droplets still dominate the concentration data for the larger sizes.

6. Discussion

[66] Figures 10 and 12 show that V_{eff} is much smaller than the candidate production velocities $U_{A_{1/3}}$ and V_{ej} for the smallest droplets in our data set: droplets with r_0 less than 10–20 μm. Figures 3 and 5 help explain this result. For these smaller droplets, gravitational settling and turbulent deposition are simply too slow to offset surface production. In other words, droplets in this size range were not produced locally; hence, the C_0 values in Figure 2 are too large to be closely associated with local production. Consequently, the V_{eff} values implied by these concentration data are too small.

[67] A caveat of this conclusion is that the near-equality between σ_{wd} and V_{eff} (Figure 11) for radii smaller than $r_0 = 10$ μm is a coincidence. Because the calculated V_{eff} in this range is not a meaningful production velocity, a simple velocity parameter like σ_{wd} cannot explain it.

[68] For droplet radii less than 20 μm, our spray generation function is or is closely related to the *Monahan et al.* [1986] function [*Andreas*, 1992, 2002]. *Monahan et al.* [1986] obtained the size distribution and production rate for droplets in this range from a laboratory whitecap simulation tank. Before creating a whitecap in their tank, they pumped all of the residual droplets out of the head space and, therefore, knew that droplets they observed were produced in the new whitecap. As a result, we know that, in the size range $r_0 < 20$ μm, the dF/dr_0 that we use in (5) to estimate V_{eff} is the rate at which bubble-derived droplets are produced locally.

[69] For naturally produced small droplets, however, the local concentration at an observation site results from the accumulated production and removal over the last day in an air mass that may have traveled several hundred kilometers. Moreover, because spray production is highly nonlinear with wind speed, the measured mean droplet concentration will be greater than the concentration predicted by the local mean wind speed. The net effect is that nonlocally produced droplets included in the observations of droplet concentration, C_0 in (5), would make V_{eff} unnaturally small.

[70] The inevitable conclusion is that no candidate velocity exists that satisfies the model

$$\frac{dF/dr_0}{V_{can}} = C_0(r_0) \tag{22}$$

in the size range $r_0 < 20$ μm.

[71] For droplets with $r_0 > 20$ μm, on the other hand, both $U_{A_{1/3}}$ and V_{ej} seem to be reasonable candidates for V_{can} in

(22). Choosing $U_{A_{1/3}}$ makes physical sense because the steep wavefront ahead of the crest of a breaking wave converts $U_{A_{1/3}}$ into a vertical wind component of comparable magnitude that clearly lifts droplets away from the surface.

[72] Meanwhile, V_{ej} explicitly models the upward velocity only of jet droplets. Perhaps the similarity between V_{ej} and V_{eff} in Figure 12 for the larger droplets is merely fortuitous. Or maybe wind speeds were low enough in our data set that jet droplet production dominated spume production. We cannot expect jet production to continue dominating in higher winds, whereas $U_{A_{1/3}}$ should still be a reliable production velocity in higher winds.

[73] Throughout our analysis, we assumed that the droplet sizes reported by the sources in Table 1 are radii at formation, r_0. Figures 3 and 5, however, suggest that the smaller droplets in our study may have been at or near r_{eq}, the equilibrium radius in the given conditions. From the discussion above, in which we concluded that the model (22) is not relevant for droplets with r_0 less than 20 μm, the assumption about the reported droplet size would not alter our findings.

[74] From Figures 3 and 5, we can also conclude that, for the largest droplets in our study, the assumption that the observed droplets still had radii at or very near r_0 is good. The turbulence simply was not able to keep these large droplets suspended long enough for them to change radius very much.

[75] For intermediate-size droplets, say, those assumed to have r_0 values between 20 and 50 μm, ambiguity remains over their size when they were observed. The effects of this ambiguity on dF/dr_0 and $C_0(r_0)$ are compensating, however; hence, calculated values of V_{eff} change little. If the observed droplet radius, r, is the result of evaporation for a droplet with initial radius r_0, the two radii are functionally related [e.g., *Andreas*, 1990, 2005a]; say,

$$r = f(r_0, T, RH, S), \tag{23}$$

where f is a known function of r_0, air temperature T, relative humidity RH, and sea surface salinity S.

[76] Hence, to find V_{eff} from (5), instead of evaluating dF/dr_0 at r (i.e., dF/dr under the original assumption that r is r_0), we would need to evaluate it at r_0 as computed from (23). Because this radius is always larger than r, the new dF/dr_0 is always smaller that dF/dr (see Figure 1). The difference will depend on r and r_0; but because r_0 is never more than four times larger than r [e.g., *Andreas*, 2002], over the r_0 range 10 to 100 μm, dF/dr_0 will never decrease by more than a factor of 8 (Figure 1).

[77] But C_0 must similarly decrease. To get the true $C_0(r_0)$ from the observed $C_0(r)$, we convert using (23), as in (6) and (7) [cf. *Andreas*, 2002]:

$$C_0(r_0) = \frac{dr}{dr_0} C_0(r). \tag{24}$$

Here, dr/dr_0 is always less than one and is approximately r/r_0.

[78] The upshot of these conversions is that the effective velocity based on the assumption that r is r_0 is not much different than the corrected velocity:

$$V_{eff}(r) = \frac{dF/dr}{C_0(r)} \approx \frac{dF/dr_0}{C_0(r_0)} = V_{eff}(r_0). \tag{25}$$

Consequently, the V_{eff} values in Figure 8, for example, are still approximately correct for $20 \le r_0 \le 50$ μm; the appropriate radius for the depicted value might be somewhat larger, however.

[79] Of course, using a different radius will also affect our computations of some of the candidate velocities that appear in the V_{can}/V_{eff} plots, Figures 9–12. Right away, though we know that ambiguity in droplet size did not affect our discussion of $U_{A_{1/3}}$ or σ_{wd} as the candidate velocity: $U_{A_{1/3}}$ is independent of droplet size, and σ_{wd} has negligible size dependence for our sizes of concern.

[80] The deposition velocity, V_{Dh}, and the ejection velocity, V_{ej}, are strongly size dependent, however. Nevertheless, in the radius range of most concern, 20–50 μm, V_{Dh} (Figure 4) would increase by a factor of 8–10 for a maximum factor-of-four radius increase; and V_{ej} might decrease by a factor of 4–5. Even these maximum ranges of potential changes would not alter our interpretations of V_{Dh}/V_{eff} and V_{ej}/V_{eff} in Figures 9 and 12, respectively. The size uncertainty for droplets with r_0 in the range 20–50 μm does not seem to have a large enough effect to change our original conclusions about V_{can}/V_{eff}.

7. Conclusions

[81] Dimensional analysis suggests that the surface production rate of sea spray droplets with initial radius r_0, dF/dr_0, should be related to the near-surface concentration of the droplets, $C_0(r_0)$, through an effective production velocity. Using a reasonable model for dF/dr_0 and 13 suitable sets of observations of $C_0(r_0)$, we have computed estimates of this effective production velocity, $V_{eff}(r_0)$, for radii r_0 between 5 and 300 μm. The results have implications for inferring dF/dr_0 from measurements of C_0 and for calculating the near-surface spray concentration profile, $C(z,r_0)$, from a model for dF/dr_0.

[82] We evaluated four candidate models for the effective production velocity: the deposition velocity at height $H_{1/3}/2$ (= $A_{1/3}$), V_{Dh}; the mean wind speed at height $H_{1/3}/2$, $U_{A_{1/3}}$; the standard deviation in the turbulence-driven vertical droplet velocity, σ_{wd}; and the measured ejection velocity of jet droplets, V_{ej}. $U_{A_{1/3}}$ and V_{ej} were the candidate models closet to the calculated values of V_{eff}. $U_{A_{1/3}}$ agreed with V_{eff} to within a factor of five for almost all $r_0 \ge 20$ μm. V_{ej} likewise agreed with V_{eff} to within a factor of about five over this same radius range and was best at explaining the radius dependence of V_{eff} in this size range. This good result with V_{ej} suggests that spume droplets do not dominate the concentration data yet for radii between 20 and 300 μm and for wind speeds up to 20 m s^{-1}.

[83] V_{Dh}, the standard model for relating dF/dr_0 and $C_0(r_0)$, typically under predicted V_{eff} by 1–2 orders of magnitude. Only for the largest droplets, $r_0 > 150$ μm, was V_{Dh} within a factor of 10 of the calculated V_{eff} values. This result implies that the assumption of equilibrium that underlies (3) and (4) is not valid and, furthermore, that spray generation functions derived from (4) [e.g., *Smith et al.*, 1993; *Hoppel et al.*, 2002] are probably too small [cf. *Andreas*, 1998].

[84] The estimated standard deviation in vertical droplet velocity, σ_{wd}, also generally under predicted V_{eff}. But for

$r_0 < 20$ μm, σ_{wd} and V_{eff} were close. We presume, however, that this agreement is a coincidence.

[85] On estimating droplet residence times, we conclude that, in the marine atmospheric surface layer, the near-surface droplet concentration cannot be assumed to be in equilibrium with the spray production rate for droplets with r_0 less than about 20 μm. The residence time for these droplets, based on gravitational settling, is too long for all of them to be locally produced. Because of the nonlinear wind speed dependence of surface production, all estimates of effective production velocity computed as $(dF/dr_0)/C_0(r_0)$ are likely to be biased low. The inevitable conclusion is that, for droplets with radii less than about 20 μm, dF/dr_0 and $C_0(r_0)$ cannot be related through any simple local velocity scale.

[86] For droplets larger than 20 μm, we recommend $U_{A_{1/3}}$ as the velocity scale for relating dF/dr_0 and $C_0(r_0)$. Although the ejection velocity of jet droplets, V_{ej}, produced results comparable to $U_{A_{1/3}}$ for our data set, we do not expect V_{ej} to still be meaningful in higher winds when spume production dominates jet droplet production for $r_0 > 20$ μm. $U_{A_{1/3}}$, on the other hand, should still be a physically meaningful velocity scale.

[87] Our analysis has been unable, however, to reduce the uncertainty in dF/dr_0 for large droplets (again, $r_0 > 20$ μm). For these droplets, $U_{A_{1/3}}$ and the computed V_{eff} values agree to within about half an order of magnitude. This is still the typical uncertainty in estimates of dF/dr_0.

Appendix A: Derivation of the Deposition Velocity

[88] The conservation equation for the number concentration C(r) of droplets with radius r is [e.g., *Fairall et al.*, 1990, 2009]

$$\frac{DC}{Dt} = -\frac{\partial F_z}{\partial z}. \tag{A1}$$

Here, D/Dt is the material derivative, and F_z is the vertical flux of droplets of radius r at height z:

$$F_z = \overline{wc} - D_d\frac{\partial C}{\partial z} - V_g C + \overline{w_s c} + S_c. \tag{A2}$$

In this, w and c are turbulent fluctuations in vertical velocity and droplet concentration, the overbar denotes a time average, $\partial C/\partial z$ is the vertical gradient in mean droplet concentration, D_d is the molecular diffusion coefficient in air of droplets with radius r, V_g is the terminal fall speed (always positive in our convention), w_s is the fluctuation in air-droplet slip velocity, and S_c ($\equiv dF/dr|_z$) is the source function at height z for droplets of radius r.

[89] This S_c has units of number of droplets of radius r moving upward at height z per square meter per second. It can be obtained from the volume source function Q_c, which has units of droplets of radius r created at height z per cubic meter per second. That is, S_c comes from Q_c as follows:

$$S_c(z) = \int_z^\infty Q_c(z')dz'. \tag{A3}$$

[90] The slip velocity, w_s in (A2), is the difference between the vertical wind velocity w and the droplet's vertical velocity. Large droplets can have a significant mean slip velocity because of gravitational settling. Although fluctuations in slip velocity average to zero, they may have nonzero correlation with wind velocity fluctuations, especially near the surface where inertia may cause droplets to deviate from the highly curved streamlines.

[91] When the concentration of droplets of radius r is near equilibrium, (A1) implies that F_z is constant with height. Call this constant $F_z = F$.

[92] We estimate the two covariance terms in (A2) from surface-layer similarity theory:

$$\overline{wc} = -K(z)\frac{\partial C}{\partial z}, \tag{A4a}$$

$$\overline{w_s c} = -\gamma u_* \, C. \tag{A4b}$$

Here, K(z) is the eddy diffusivity; γ is a coefficient defined below; and u_* is the friction velocity and, as usual, is assumed to be constant with height.

[93] The slip term $\overline{w_s c}$ represents how droplet inertia prevents the droplets from perfectly following the turbulent air, which has turbulent vertical velocity w. Following *Fairall and Larsen* [1984], we parameterize γ as

$$\gamma = \frac{C_{Dr}^{1/2}}{k} 10^{-3/St}, \tag{A5}$$

where C_{Dr} is the drag coefficient at reference height r (usually 10 m) and k is still the von Kármán constant. Also in (A5),

$$St = \frac{V_g u_*^2}{\nu g} \tag{A6}$$

is the Stokes parameter, where ν is the kinematic viscosity of air and g is the acceleration of gravity.

[94] Substituting (A4) into (A2) yields

$$F = -[D_d + K(z)]\frac{\partial C}{\partial z} - \left(V_g + \gamma u_*\right)C + S_c. \tag{A7}$$

We can solve this differential equation in C(z) with the transformation

$$M(z, r) = C(z, r) + \frac{F - S_c}{V_g + \gamma u_*}. \tag{A8}$$

[95] Because the $(F - S_c)/(V_g + \gamma u_*)$ term is constant with height, we can rewrite (A7) as

$$M = -\left(\frac{D_d + K(z)}{V_g + \gamma u_*}\right)\frac{\partial M}{\partial z} \tag{A9}$$

or

$$\frac{1}{M}\frac{\partial M}{\partial z} = -\frac{V_g + \gamma u_*}{D_d + K(z)}. \tag{A10}$$

This has the formal solution

$$\ln\left[\frac{M(z, r)}{M(0, r)}\right] = -\int_0^z \frac{V_g + \gamma u_*}{D_d + K(z')}dz' \equiv I_z. \tag{A11}$$

[96] *Fairall et al.* [2000] show how to evaluate the integral under the assumption that

$$K(z) = \frac{ku_* z}{1 + \frac{\delta}{z}}. \tag{A12}$$

Here, δ is the thickness of the molecular sublayer for droplets at the sea surface; it is

$$\delta = \lambda \frac{\nu}{u_*}, \tag{A13}$$

where $\lambda \approx 25$. Then

$$ku_* I_z = \ln(z/\delta) + \ln(k\lambda Sc)^{1/2} + \frac{\pi}{2}(k\lambda Sc)^{1/2} \tag{A14a}$$

$$= \ln(z/\delta) + R_p. \tag{A14b}$$

Here, $Sc = \nu/D_d$ is the droplet Schmidt number and is assumed to be very large. Equation (A14) also defines R_p, which parameterizes droplet transport by Brownian diffusion.

[97] On combining (A11) and (A14b), we obtain

$$\ln\left[\frac{M(z,r)}{M(0,r)}\right] = -\frac{V_g + \gamma u_*}{ku_*}\left[\ln\left(\frac{z}{\delta}\right) + R_p\right]. \tag{A15}$$

Using (A8) but assuming for the moment that there is no source of droplets (i.e., $S_c = 0$), we evaluate (A15) in two layers. In layer I, $z \le \delta$ and γ is nonzero. In layer II, $z \ge \delta$ and γ is zero.

[98] In layer I, from (A8),

$$M(z,r) = C(z,r) + \frac{F}{V_g + \gamma u_*} \tag{A16a}$$

and

$$M(0,r) = C(0,r) + \frac{F}{V_g + \gamma u_*}. \tag{A16b}$$

Consequently, from (A15),

$$\frac{M(z,r)}{M(0,r)} = \frac{C_z + \frac{F}{V_g + \gamma u_*}}{C_0 + \frac{F}{V_g + \gamma u_*}} = \exp\left\{-\frac{V_g + \gamma u_*}{ku_*}\left[\ln\left(\frac{z}{\delta}\right) + R_p\right]\right\}, \tag{A17}$$

where we have abbreviated C(z,r) as C_z and C(0,r) as C_0.

[99] At $z = \delta$,

$$\frac{C_\delta + \frac{F}{V_g + \gamma u_*}}{C_0 + \frac{F}{V_g + \gamma u_*}} = f_{0\delta}, \tag{A18}$$

where $C_\delta \equiv C(\delta,r)$ and

$$f_{0\delta} \equiv \exp\left[-\frac{(V_g + \gamma u_*)R_p}{ku_*}\right]. \tag{A19}$$

Solving (A18) for the (constant) droplet flux, we obtain

$$F = -(V_g + \gamma u_*)\left(C_0 + \frac{C_\delta - C_0}{1 - f_{0\delta}}\right). \tag{A20}$$

[100] In layer II, where $\gamma = 0$, we can evaluate M(z,r) at δ and at some height $z > \delta$ as

$$\ln\left[\frac{M(\delta,r)}{M(0,r)}\right] = -\frac{V_g R_p}{ku_*} \tag{A21a}$$

and

$$\ln\left[\frac{M(z,r)}{M(0,r)}\right] = -\frac{V_g}{ku_*}\left[\ln\left(\frac{z}{\delta}\right) + R_p\right]. \tag{A21b}$$

Therefore,

$$\ln\left[\frac{M(z,r)}{M(\delta,r)}\right] = -\frac{V_g}{ku_*}\ln\left(\frac{z}{\delta}\right). \tag{A22}$$

Consequently, from (A8), still with $S_c = 0$,

$$\frac{C_z + \frac{F}{V_g}}{C_0 + \frac{F}{V_g}} = f_{\delta z}, \tag{A23}$$

where

$$f_{\delta z} \equiv \exp\left[-\frac{V_g}{ku_*}\ln\left(\frac{z}{\delta}\right)\right] = \left(\frac{z}{\delta}\right)^{-V_g/ku_*}. \tag{A24}$$

[101] Equation (A23) leads to another expression for the droplet flux:

$$F = -V_g\left(C_\delta + \frac{C_z - C_\delta}{1 - f_{\delta z}}\right). \tag{A25}$$

[102] For the case of pure deposition and with the assumption that the surface is a pure sink such that $C_0 = 0$ [*Giorgi*, 1986], we can eliminate C_δ from (A20) and (A25) to obtain the deposition velocity. First, though, rewrite (A20) as

$$F = -\frac{(V_g + \gamma u_*)C_\delta}{1 - f_{0\delta}}. \tag{A26}$$

Notice here that

$$\frac{V_g + \gamma u_*}{1 - \exp\left[-\frac{(V_g + \gamma u_*)R_p}{ku_*}\right]} \approx V_g + \gamma u_* + \frac{ku_*}{R_p}. \tag{A27}$$

We can make this approximation because $(V_g + \gamma u_*)R_p/ku_*$ is large and $\exp[-(V_g + \gamma u_*)R_p/ku_*]$ is, therefore, much less than one.

[103] Equation (A26) thus becomes

$$F = -\left(V_g + \gamma u_* + \frac{ku_*}{R_p}\right)C_\delta. \tag{A28}$$

Substituting C_δ from this into (A25) then yields

$$F = -\frac{V_g + V_a}{1 + \frac{V_a}{V_g}(1 - f_{\delta z})} C_z, \tag{A29}$$

where

$$V_a \equiv \gamma u_* + \frac{k u_*}{R_p}. \tag{A30}$$

The quantity

$$V_{Dz} \equiv -\frac{V_g + V_a}{1 + \frac{V_a}{V_g}(1 - f_{\delta z})} \tag{A31}$$

is the deposition velocity at height z because it relates the droplet concentration at z to the (constant) downward flux of droplets.

[104] The one quantity that we have not discussed yet is the droplet diffusivity, D_d. *Pruppacher and Klett* [1978, p. 361] give

$$D_d = \frac{\kappa\, T(1 + \alpha\, Kn)}{6\pi\rho\nu r}, \tag{A32}$$

where κ (=1.380650 × 10^{-23} J K^{-1}) is the Boltzmann constant, T is the absolute temperature, ρ is the air density, and r is the droplet radius. Also in (A32), Kn is the Knudsen number,

$$Kn = \frac{\lambda_a}{r}, \tag{A33}$$

where λ_a is the mean free path of air molecules [*Andreas*, 2005b]; and [*Pruppacher and Klett*, 1978, p. 361]

$$\alpha = 1.257 + 0.400 \exp\left[-\frac{1.10}{Kn}\right]. \tag{A34}$$

[105] Next, we consider including the spray generation function, S_c, in our analysis. Our conceptual picture is that spray generation occurs close to the surface at $0 < z \le h$, where we will eventually take h as the significant wave amplitude, $h = H_{1/3}/2$. In this layer, S_c is independent of height [cf. *Iida et al.*, 1992; *Fairall et al.*, 2009]. This is essentially the assumption that we made to obtain (A9). Above h, there is no source; so $S_c = 0$ here. Thus, (A9) is still accurate in this region but with S_c set to zero.

[106] With this interpretation of S_c, (A20) becomes

$$F - S_c = -\left(V_g + \gamma u_*\right)\left(C_0 + \frac{C_\delta - C_0}{1 - f_{0\delta}}\right). \tag{A35}$$

Likewise, when we replace z with h, (A25) becomes

$$F - S_c = -V_g\left(C_\delta + \frac{C_h - C_\delta}{1 - f_{\delta h}}\right), \tag{A36}$$

where $C_h \equiv C(h, r)$ is the droplet concentration at height h. Because the surface sink is still perfect, C_0 is still zero; and (A35) and (A36) lead to a solution like (A29):

$$F - S_c = -\frac{V_g + V_a}{1 + \frac{V_a}{V_g}(1 - f_{\delta h})} C_h. \tag{A37}$$

[107] Thus, even with a droplet source, the effective deposition velocity at z = h still has the same form as (A31). This expression for deposition velocity is therefore what we use in (10). This development also explains why we focus on the measured droplet concentrations at low level: We require C_h, the droplet concentration at the approximate amplitude of the significant waves.

[108] **Acknowledgments.** We thank two anonymous reviewers for suggestions that helped clarify our presentation. The U.S. Mineral Management Service supported this work under Interagency Agreement M07RG13274. The U.S. Office of Naval Research also supported ELA through grant N00014-08-1-0411.

References

Andreas, E. L (1990), Time constants for the evolution of sea spray droplets, *Tellus, Ser. B*, *42*, 481–497, doi:10.1034/j.1600-0889.1990.t01-3-00007.x.

Andreas, E. L (1992), Sea spray and the turbulent air-sea heat fluxes, *J. Geophys. Res.*, *97*, 11,429–11,441, doi:10.1029/92JC00876.

Andreas, E. L (1998), A new sea spray generation function for wind speeds up to 32 m s^{-1}, *J. Phys. Oceanogr.*, *28*, 2175–2184, doi:10.1175/1520-0485(1998)028<2175:ANSSGF>2.0.CO;2.

Andreas, E. L (2002), A review of the sea spray generation function for the open ocean, in *Atmosphere-Ocean Interactions*, vol. 1, edited by W. Perrie, pp. 1–46, WIT, Southampton, U. K.

Andreas, E. L (2004), Spray stress revisited, *J. Phys. Oceanogr.*, *34*, 1429–1440, doi:10.1175/1520-0485(2004)034<1429:SSR>2.0.CO;2.

Andreas, E. L (2005a), Approximation formulas for the microphysical properties of saline droplets, *Atmos. Res.*, *75*, 323–345, doi:10.1016/j.atmosres.2005.02.001.

Andreas, E. L (2005b), *Handbook of Physical Constants and Functions for Use in Atmospheric Boundary Layer Studies*, *ERDC/CRREL Monogr. M-05-1*, 42 pp., U.S. Army Cold Reg. Res. and Eng. Lab., Hanover, N. H.

Andreas, E. L (2010), Spray-mediated enthalpy flux to the atmosphere and salt flux to the ocean in high winds, *J. Phys. Oceanogr.*, *40*, 608–619, doi:10.1175/2009JPO4232.1.

Andreas, E. L, and J. DeCosmo (1999), Sea spray production and influence on air-sea heat and moisture fluxes over the open ocean, in *Air-Sea Exchange: Physics, Chemistry and Dynamics*, edited by G. L. Geernaert, pp. 327–362, Kluwer, Dordrecht, Netherlands.

Andreas, E. L, and S. Wang (2007), Predicting significant wave height off the northeast coast of the United States, *Ocean Eng.*, *34*, 1328–1335, doi:10.1016/j.oceaneng.2006.08.004.

Andreas, E. L, J. B. Edson, E. C. Monahan, M. P. Rouault, and S. D. Smith (1995), The spray contribution to net evaporation from the sea: A review of recent progress, *Boundary Layer Meteorol.*, *72*, 3–52, doi:10.1007/BF00712389.

Andreas, E. L, M. J. Pattison, and S. E. Belcher (2001), "Production rates of sea-spray droplets" by M. J. Pattison and S. E. Belcher: Clarification and elaboration, *J. Geophys. Res.*, *106*, 7157–7161, doi:10.1029/2000JC000233.

Andreas, E. L, P. O. G. Persson, and J. E. Hare (2008), A bulk turbulent air-sea flux algorithm for high-wind, spray conditions, *J. Phys. Oceanogr.*, *38*, 1581–1596, doi:10.1175/2007JPO3813.1.

Blanchard, D. C. (1963), The electrification of the atmosphere by particles from bubbles in the sea, *Prog. Oceanogr.*, *1*, 71–202, doi:10.1016/0079-6611(63)90004-1.

Burk, S. D. (1984), The generation, turbulent transfer and deposition of the sea-salt aerosol, *J. Atmos. Sci.*, *41*, 3040–3051, doi:10.1175/1520-0469(1984)041<3040:TGTTAD>2.0.CO;2.

DeCosmo, J. (1991), Air-sea exchange of momentum, heat and water vapor over whitecap sea states, Ph.D. thesis, 212 pp., Univ. of Wash., Seattle.

Dekker, H., and G. de Leeuw (1993), Bubble excitation of surface waves and aerosol droplet production: A simple dynamical model, *J. Geophys. Res.*, *98*, 10,223–10,232, doi:10.1029/93JC00344.

de Leeuw, G. (1986a), Vertical profiles of giant particles close above the sea surface, *Tellus, Ser. B*, *38*, 51–61, doi:10.1111/j.1600-0889.1986.tb00087.x.

de Leeuw, G. (1986b), Size distribution of giant aerosol particles close above sea level, *J. Aerosol Sci.*, *17*, 293–296, doi:10.1016/0021-8502(86)90088-1.

de Leeuw, G. (1987), Near-surface particle size distribution profiles over the North Sea, *J. Geophys. Res.*, *92*, 14,631–14,635, doi:10.1029/JC092iC13p14631.

de Leeuw, G. (1990), Profiling of aerosol concentrations, particle size distributions and relative humidity in the atmospheric surface layer over the North Sea, *Tellus, Ser. B*, *42*, 342–354.

Edson, J. B., and C. W. Fairall (1994), Spray droplet modeling: 1. Lagrangian model simulation of the turbulent transport of evaporating droplets, *J. Geophys. Res.*, *99*, 25,295–25,311, doi:10.1029/94JC01883.

Fairall, C. W., and S. E. Larsen (1984), Dry deposition, surface production and dynamics of aerosols in the marine boundary layer, *Atmos. Environ.*, *18*, 69–77, doi:10.1016/0004-6981(84)90229-4.

Fairall, C. W., K. L. Davidson, and G. E. Schacher (1984), Application of a mixed-layer model to aerosols in the marine boundary layer, *Tellus, Ser. B*, *36*, 203–211, doi:10.1111/j.1600-0889.1984.tb00242.x.

Fairall, C. W., J. B. Edson, and M. A. Miller (1990), Heat fluxes, whitecaps, and sea spray, in *Surface Waves and Fluxes*, vol. 1, edited by G. L. Geernaert and W. J. Plant, pp. 173–208, Kluwer, Dordrecht, Netherlands.

Fairall, C. W., J. D. Kepert, and G. J. Holland (1994), The effect of sea spray on surface energy transports over the ocean, *Global Atmos. Ocean Syst.*, *2*, 121–142.

Fairall, C. W., J. E. Hare, J. B. Edson, and W. McGillis (2000), Parameterization and micrometeorological measurement of air-sea gas transfer, *Boundary Layer Meteorol.*, *96*, 63–105, doi:10.1023/A:1002662826020.

Fairall, C. W., M. L. Banner, W. L. Pierson, W. Asher, and R. P. Morison (2009), Investigation of the physical scaling of sea spray spume droplet production, *J. Geophys. Res.*, *114*, C10001, doi:10.1029/2008JC004918.

Garratt, J. R. (1992), *The Atmospheric Boundary Layer*, 316 pp., Cambridge Univ. Press, Cambridge, U. K.

Giorgi, F. (1986), A particle dry-deposition parameterization scheme for use in tracer transport models, *J. Geophys. Res.*, *91*, 9794–9806, doi:10.1029/JD091iD09p09794.

Gong, S. L. (2003), A parameterization of sea-salt aerosol source function for sub- and super-micron particles, *Global Biogeochem. Cycles*, *17*(4), 1097, doi:10.1029/2003GB002079.

Gong, S. L., L. A. Barrie, and J.-P. Blanchet (1997), Modeling sea-salt aerosols in the atmosphere. 1. Model development, *J. Geophys. Res.*, *102*, 3805–3818, doi:10.1029/96JD02953.

Goroch, A., S. Burk, and K. L. Davidson (1980), Stability effects on aerosol size and height distributions, *Tellus*, *32*, 245–250, doi:10.1111/j.2153-3490.1980.tb00951.x.

Hoppel, W. A., G. M. Frick, and J. W. Fitzgerald (2002), Surface source function for sea-salt aerosol and aerosol dry deposition to the ocean surface, *J. Geophys. Res.*, *107*(D19), 4382, doi:10.1029/2001JD002014.

Hoppel, W. A., P. F. Caffrey, and G. M. Frick (2005), Particle deposition on water: Surface source versus upwind source, *J. Geophys. Res.*, *110*, D10206, doi:10.1029/2004JD005148.

Iida, N., Y. Toba, and M. Chaen (1992), A new expression for the production rate of sea water droplets on the sea surface, *J. Oceanogr.*, *48*, 439–460, doi:10.1007/BF02234020.

Jones, K. F., and E. L Andreas (2009), Sea spray icing of drilling and production platforms, *ERDC/CRREL Tech. Rep. TR-09-03*, 54 pp., U.S. Army Cold Reg. Res. and Eng. Lab., Hanover, N. H.

Kaimal, J. C., and J. J. Finnigan (1994), *Atmospheric Boundary Layer Flows: Their Structure and Measurement*, 289 pp., Oxford Univ. Press, New York.

Kind, R. J. (1992), One-dimensional aeolian suspension above beds of loose particles—A new concentration-profile relation, *Atmos. Environ.*, *26A*, 927–931.

Kinsman, B. (1965), *Wind Waves*, 676 pp., Prentice-Hall, Englewood Cliffs, N. J.

Lewis, E. R., and S. E. Schwartz (2004), *Sea Salt Aerosol Production: Mechanisms*, *Methods*, *Measurements*, *and Models—A Critical Review*, 413 pp., AGU, Washington, D. C.

Lewis, E. R., and S. E. Schwartz (2006), Comment on "Size distribution of sea-salt emissions as a function of relative humidity," *Atmos. Environ.*, *40*, 588–590, doi:10.1016/j.atmosenv.2005.08.043.

Massel, S. R. (2007), *Ocean Waves Breaking and Marine Aerosol Fluxes*, 323 pp., Springer, New York.

Meek, C. C., and B. G. Jones (1973), Studies of the behavior of heavy particles in a turbulent fluid flow, *J. Atmos. Sci.*, *30*, 239–244, doi:10.1175/1520-0469(1973)030<0239:SOTBOH>2.0.CO;2.

Monahan, E. C. (1968), Sea spray as a function of low elevation wind speed, *J. Geophys. Res.*, *73*, 1127–1137, doi:10.1029/JB073i004p01127.

Monahan, E. C., C. W. Fairall, K. L. Davidson, and P. J. Boyle (1983), Observed inter-relations between 10 m winds, ocean whitecaps and marine aerosols, *Q. J. R. Meteorol. Soc.*, *109*, 379–392, doi:10.1002/qj.49710946010.

Monahan, E. C., D. E. Spiel, and K. L. Davidson (1986), A model of marine aerosol generation via whitecaps and wave disruption, in *Oceanic Whitecaps and Their Role in Air-Sea Exchange Processes*, edited by E. C. Monahan and G. Mac Niocaill, pp. 167–174, D. Reidel, Dordrecht, Netherlands.

Moore, D. J., and B. J. Mason (1954), The concentration, size distribution and production rate of large salt nuclei over the oceans, *Q. J. R. Meteorol. Soc.*, *80*, 583–590, doi:10.1002/qj.49708034607.

Mueller, J. A., and F. Veron (2009a), A Lagrangian stochastic model for heavy particle dispersion in the atmospheric marine boundary layer, *Boundary Layer Meteorol.*, *130*, 229–247, doi:10.1007/s10546-008-9340-8.

Mueller, J. A., and F. Veron (2009b), A sea state dependent spume generation function, *J. Phys. Oceanogr.*, *39*, 2363–2372, doi:10.1175/2009JPO4113.1.

Panofsky, H. A., and J. A. Dutton (1984), *Atmospheric Turbulence: Models and Methods for Engineering Applications*, 397 pp., John Wiley, New York.

Pattison, M. J., and S. E. Belcher (1999), Production rates of sea-spray droplets, *J. Geophys. Res.*, *104*, 18,397–18,407, doi:10.1029/1999JC900090.

Preobrazhenskii, L. Y. (1973), Estimate of the content of spray-drops in the near-water layer of the atmosphere, *Fluid Mech. Sov. Res.*, *2*, 95–100.

Pruppacher, H. R., and J. D. Klett (1978), *Microphysics of Clouds and Precipitation*, 714 pp., D. Reidel, Dordrecht, Netherlands.

Rouault, M. P., P. G. Mestayer, and R. Schiestel (1991), A model of evaporating spray droplet dispersion, *J. Geophys. Res.*, *96*, 7181–7200, doi:10.1029/90JC02569.

Slinn, S. A., and W. G. N. Slinn (1980), Predictions for particle deposition on natural waters, *Atmos. Environ.*, *14*, 1013–1016, doi:10.1016/0004-6981(80)90032-3.

Slinn, W. G. N. (1983), Air-to-sea transfer of particles, in *Air-Sea Exchange of Gases and Particles*, edited by P. S. Liss and W. G. N. Slinn, pp. 299–405, D. Reidel, Dordrecht, Netherlands.

Slinn, W. G. N., L. Hasse, B. B. Hicks, A. W. Hogan, D. Lal, P. S. Liss, K. O. Munnich, G. A. Sehmel, and O. Vittori (1978), Some aspects of the transfer of atmospheric trace constituents past the air-sea interface, *Atmos. Environ.*, *12*, 2055–2087, doi:10.1016/0004-6981(78)90163-4.

Smith, M. H., P. M. Park, and I. E. Consterdine (1993), Marine aerosol concentrations and estimated fluxes over the sea, *Q. J. R. Meteorol. Soc.*, *119*, 809–824, doi:10.1002/qj.49711951211.

Spiel, D. E. (1994), The sizes of jet drops produced by air bubbles bursting on sea- and fresh-water surfaces, *Tellus, Ser. B*, *46*, 325–338.

Spiel, D. E. (1995), On the birth of jet drops from bubbles bursting on water surfaces, *J. Geophys. Res.*, *100*, 4995–5006, doi:10.1029/94JC03055.

Spiel, D. E. (1997), More on the births of jet drops from bubbles bursting on seawater surfaces, *J. Geophys. Res.*, *102*, 5815–5821, doi:10.1029/96JC03582.

Stull, R. B. (1988), *An Introduction to Boundary Layer Meteorology*, 666 pp., Kluwer, Dordrecht, Netherlands.

Toba, Y. (1965), On the giant sea-salt particles in the atmosphere: II. Theory of the vertical distribution in the 10-m layer over the ocean, *Tellus*, *17*, 365–382, doi:10.1111/j.2153-3490.1965.tb01429.x.

Tucker, M. J., and E. G. Pitt (2001), *Waves in Ocean Engineering*, 521 pp., Elsevier, Amsterdam.

Williams, R. M. (1982), A model for the dry deposition of particles to natural water surfaces, *Atmos. Environ.*, *16*, 1933–1938, doi:10.1016/0004-6981(82)90464-4.

Wu, J. (1982), Sea spray: A further look, *J. Geophys. Res.*, *87*, 8905–8912, doi:10.1029/JC087iC11p08905.

E. L Andreas, Seattle Division, NorthWest Research Associates, Inc., 25 Eagle Rdg., Lebanon, NH 03766, USA. (eandreas@nwra.com)

C. W. Fairall, Physical Sciences Division, NOAA Earth System Research Laboratory, 325 Broadway, Boulder, CO 80305, USA.

K. F. Jones, U.S. Army Cold Regions Research and Engineering Laboratory, 72 Lyme Rd., Hanover, NH 03755, USA.